




Article

Adsorption of Arsenic on Fe-Modified Biochar and Monitoring Using Spectral Induced Polarization

Panagiotis Kirmizakis ¹, Bassam Tawabini ¹, Omer Muhammad Siddiq ¹, Dimitrios Kalderis ²,
Dimitrios Ntarlagiannis ³ and Pantelis Soupios ^{1,*}

¹ Department of Geosciences, College of Petroleum Engineering and Geosciences, King Fahd University of Petroleum and Minerals, Dhahran 31261, Saudi Arabia; p.kirmizakis@kfupm.edu.sa (P.K.); bassamst@kfupm.edu.sa (B.T.); g201801200@kfupm.edu.sa (O.M.S.)

² Department of Electronic Engineering, Hellenic Mediterranean University, 73133 Chania, Greece; kalderis@hmu.gr

³ Department of Earth and Environmental Sciences, Rutgers University, Newark, NJ 07102, USA; dimntar@newark.rutgers.edu

* Correspondence: panteleimon.soupios@kfupm.edu.sa; Tel.: +966-13-860-2689

Abstract: This work demonstrates the potential of Fe-modified biochar for the treatment of arsenic (As) simulated wastewater and the monitoring of adsorption in real-time. Specifically, we propose the utilization of date-palm leaves for the production of biochar, further modified with Fe in order to improve its adsorption function against inorganic pollutants, such as As. Both the original biochar and the Fe-modified biochar were used for adsorption of As in laboratory batch and column experiments. The monitoring of the biochar(s) performance and As treatment was also enhanced by using the spectral induced polarization (SIP) method, offering real-time monitoring, in addition to standard chemical monitoring. Both the original and the Fe-modified biochar achieved high removal rates with Fe-modified biochar achieving up to 98% removal of As compared to the 17% by sand only (control). In addition, a correlation was found between post-adsorption measurements and SIP measurements.

Keywords: biochar; arsenate; wastewater; spectral induced polarization



Citation: Kirmizakis, P.; Tawabini, B.; Siddiq, O.M.; Kalderis, D.; Ntarlagiannis, D.; Soupios, P. Adsorption of Arsenic on Fe-Modified Biochar and Monitoring Using Spectral Induced Polarization. *Water* **2022**, *14*, 563. <https://doi.org/10.3390/w14040563>

Academic Editor: Yongchang Sun

Received: 24 January 2022

Accepted: 11 February 2022

Published: 13 February 2022

Publisher's Note: MDPI stays neutral with regard to jurisdictional claims in published maps and institutional affiliations.



Copyright: © 2022 by the authors. Licensee MDPI, Basel, Switzerland. This article is an open access article distributed under the terms and conditions of the Creative Commons Attribution (CC BY) license (<https://creativecommons.org/licenses/by/4.0/>).

1. Introduction

In Saudi Arabia, freshwater sources are scarce. The supply of water largely depends on extraction from non-renewable groundwater aquifers and seawater desalination to meet the increasing demand for municipal, agricultural, and industrial uses [1,2]. Protecting these limited sources from contamination is of prime concern to the water authorities. Arsenic (As) is a hazardous contaminant regulated and monitored by local water authorities [3]. It is considered a significant threat to human health and is listed by the World Health Organization (WHO) as a Class-I carcinogen with the threshold limit in drinking water set at $10 \mu\text{g L}^{-1}$ [4]. Sources of As contamination in groundwater are diverse, and the majority of other contaminants can either be man-made or of natural origin. Several countries with elevated concentrations in their groundwater closely monitor As levels [5,6]. It is estimated that around 230 million people are affected by arsenic-contaminated drinking water [7].

Arsenic in water can be found mainly in two different redox forms, arsenate (As(V)) and arsenite (As(III)), which differ in mobilization and toxicity [8]. In anoxic environments, As is mainly present in the form of As(III); whereas in oxic environments, As(III) is oxidized to As(V) [9]. Ion exchange, adsorption, oxidation, coagulation-flocculation, and membrane separation to remove As from groundwater have been investigated [10]. Most of these technologies have several short comings related to efficiency and cost [11–14]. Studies have shown that biomass-based adsorbents can be easily and reproducibly prepared, show excellent adsorption performance, and can be recovered and reused in subsequent runs [15,16]. The mechanisms involved in As adsorption by porous materials have been thoroughly

reviewed and established [15,17,18]. Conventional adsorbents such as carbonaceous materials and fly ash, have exhibited a positive adsorption behaviour, but this is towards As(V) rather than As(III), which is highly toxic and mobile compared to As(V) [19,20].

Biochar is a porous, solid residue of biomass pyrolysis generated at high temperatures, between 300 °C and 800 °C [21]. The production conditions, mainly temperature, heating rate and residence time, and the initial biomass composition, determine the physicochemical properties of the product [22]. The behavior and efficiency of biochar in various applications, such as soil nutrient enhancement, soil remediation [23], and wastewater treatment, are determined from those properties [24]. Biochar is utilized in wastewater treatment as a reusable adsorbent or a substrate to produce catalysts for the oxidative destruction of organic compounds. Its environmental applications are driven by the properties, which in turn are determined by the feedstock material utilized and the conditions under which it is pyrolyzed. Biochar and biochar-based composite materials have demonstrated their adsorption performance in a wide range of organic and inorganic contaminants, such as As, Cd and organics such as PAHs [25]. Recently, Chen et al. demonstrated the efficiency of Fe/Mn-modified biochar to remove As (III) [26]. At a starting concentration of 1 mg/L As, the group achieved removal of 81% at pH 3. Using Fe-modified biochar, Navarathna et al. [27] achieved As removal below WHO's limit for wastewater discharge (0.2 mg/L) starting from an initial concentration of 10 mg/L at 25 °C and pH 8. Similarly, Park et al. deposited Zn on biochar and achieved a near-complete As removal (starting As concentration of 100 mg/L) at pH 6 and adsorbent dosage of 8 g/L [28]. Interestingly, the authors suggested that metal-impregnated biochars or biochar with a high naturally-occurring metal concentration show a better adsorption behaviour towards As. Most studies involving biochars and contaminants in aqueous solutions are laboratory-based, whereas results from pilot-scale remediation are limited [29]. Biochars immobilize contaminants by physical adsorption on their porous network, precipitation as insoluble carbonates/phosphates and/or electrostatic interactions (H-bonding, complexation) between the biochar surface functional groups and a charged part of the contaminant. Previous research has investigated the range of electrostatic interactions between biochar/biochar-based catalysts and pollutants [26,30–32]. Attraction between opposite charges, inherent chemical affinity with functional groups on the biochar surface, hydrogen bonding, and cation–cation interactions have all been conclusively demonstrated to play the most important roles [33,34].

Depending on the pollutant of concern, the surface of biochar may be modified accordingly to increase its adsorption performance. In this framework, chemical and physical alterations such as steam activation, gas purging, and metal or oxide impregnation have been commonly applied [35,36]. Iron oxides such as Fe₃O₄ have been shown to form complexes with heavy metals (such as Fe-arsenate) and increase the surface electrostatic attraction, and surface precipitation [37,38]. Even with modest surface area biochars, Fe modification has been shown to considerably improve heavy metal wastewater cleanup, particularly As removal [39–42]. Furthermore, deposition of Fe₃O₄ renders the adsorbent magnetic and thus easily separable from the treated solution by using a magnet.

In wastewater treatment studies, the success of the adsorption process is measured by collecting aqueous samples at predetermined intervals and at the end of the procedure, it is followed by chromatographic or spectroscopic analysis to determine the residual concentration of the pollutants, such as arsenic and organic dyes [7,24]. In practice, this is typically time-consuming and costly, because it may necessitate many analyses for a single experimental run and extensive reagent use, in addition to the geographical and temporal limitations of point sampling. Furthermore, in field-scale remediation studies where several runs may be impractical, obtaining information during the process rather than after its conclusion would allow for treatment adjustment if and when it is needed. As a result, real-time pollutant concentration monitoring would be a significant methodological leap for wastewater treatment and soil remediation applications.

Geophysical technologies provide non-invasive, high-resolution (temporal and spatial) monitoring of a parameter directly linked to a physical property of interest. For example,

electrical methods have been extensively used to characterize contaminated land, and monitor remediation efforts [43–45]. Another well-established exploration geophysical method, spectral induced polarization (SIP), is increasingly being employed as a remediation monitoring tool in lab and field applications [46–49] because of its sensitivity to the medium's bulk and interfacial parameters and/or the pollutant under examination [50]. Kirmizakis et al. [51] presented the first-ever study of biochar, focused on environmental management, utilizing SIP as a characterization and monitoring tool. They used different fractions of biochar in inert porous media as a remediation agent for olive oil mill wastewater (OMW), a waste effluent with heavy organic load, in static laboratory columns, while monitoring the SIP responses over a period of ten days. The positive findings indicated that variations in SIP responsiveness were associated with OMW sorption on biochar, which affected its surface characteristics. These findings were very encouraging, both for the treatment of organic waste using biochar and SIP as a monitoring and characterization tool.

Therefore, the main objective of this study was to investigate the adsorption performance of Fe-modified biochar prepared from date palm leaves for the removal of As(V) from As(V)-containing simulated water, combined with real-time SIP monitoring. In this framework, the study was conducted in two phases. Phase (I) included the batch adsorption study in determining the optimum treatment conditions of As by biochar. The effect of pH, adsorbent dosage, and stirring rate were investigated. Phase (II) included the SIP monitoring of the adsorption process in pilot-scale columns under the optimum conditions determined in Phase (I).

2. Materials and Methods

2.1. Materials

As standard stock of As(V) was prepared using lab-grade As (1000 µg/mL, Ultra Scientific, North Kingstown, RI, USA) and followed by acidification with 0.1 N HNO₃ (ACS Reagent Grade, 70%, Ricca Chemical, Arlington, TX, USA). Iron nitrate (Fisher Chemical, Hampton, NH, USA, 98% purity) was used for biochar modification. HCl (Fisher Chemical 36.5–38%) and NaOH (research products international—RPI pellets) were used for pH adjustments. Ultrapure water (Milli-Q Ultrapure Type 1 water) was used for preparing stock solutions. Clean sand was employed as the porous reference material in SIP monitoring tests. This sand was washed with HNO₃, HCl, and ultrapure water (18.1 MΩ·cm) until the pH reached 7.

Dried date palm leaves (DPL) were obtained from a private farm in Khobar, Eastern Saudi Arabia, and utilized as biochar feedstock. Biochar production by DPLs has been increased in recent years due to their abundance in the Middle East and the high volume of waste produced from the cultivation of the palm trees [52]. The leaves were cleaned with distilled water, air-dried for 24 h, crushed, and sieved to a particle size of less than 1 mm. For pyrolysis, DPLs were transferred into iron column-rods (to minimize oxygen) and placed in a muffle furnace at desired temperatures (300, 500, and 800 °C) for 4 h [53]. The prepared biochars are referred to as BC300, BC500 and BC800. Following production, the biochar was sieved, and only the ≤300 µm fraction was utilized to conduct the experiments. The produced biochar was Fe-modified following the procedure of Din et al. [54]. Biochar was mixed with Fe(NO₃)₃ (High purity Lab grade) and deionized water (Milli-Q) in the ratio 10 g:7 g:250 mL. The pH of the mixture was raised to 11 using 0.1 M NaOH. The mixture was stirred overnight on a hot plate at 40 °C. Multiple washing rounds were then conducted using DI water until the pH was neutral (7). The remaining liquid was decanted, and biochar was kept for oven drying at 105 °C. The raw biochar and the Fe-functionalized sample were characterized in accordance with the European Biochar Certificate requirements (EBC). Their surface morphology was captured using scanning electron microscopy (SEM) Tescan Lyra-3. The raw and modified biochar's C, H, and N content was measured by an elemental analyzer (Perkin Elmer EA—2400). The crystalline structure was determined using XRD (Ultima IV), and reflection data was acquired as a survey scan using a Panalytical vertical diffractometer with copper K_α radiation. The

surface functional groups in raw and modified biochar before and after As adsorption were identified using FTIR spectrophotometry (Smart iTR NICOLET iS10) in the range of 4000–550 cm^{-1} .

2.2. Methods

2.2.1. Batch Adsorption Studies

Batch adsorption experiments were conducted in 50 mL conical flasks to determine the adsorption capacity of the biochar sample and highlight the influence of the most important process parameters (solution pH, adsorbent dosage) prior to the SIP-column adsorption monitoring. We used 4 g/L of biochar in all runs with varying As concentrations (0.5 to 30 mg/L). Experiments were conducted on an automatic shaker at 200 rpm under 23 °C temperature. After reaching equilibrium, the mixture was allowed to settle, and 2 mL of the sample was collected for further analysis. The samples were analyzed using ICP-OES (Plasma Quant 9000; Analytik Jena GmbH). The effect of pH on adsorption was studied at pH values of 3, 5, 7, 9, and 11. The pH of the solution (before biochar addition) was adjusted using either 0.1 M NaOH or 0.1 HNO_3 . The effect of stirring rate was investigated by repeating specific adsorption runs at various agitation speeds (i.e., 100, 150, 200, and 250 rpm). For the effect of the adsorbent dosage, 2, 4, 8, 12, 16, and 20 g/L of adsorbent was used.

2.2.2. SIP Monitoring

A preliminary geophysical investigation was done by Siddiq et al. [3] in order to correlate SIP parameters (real and imaginary conductivity) to the interactions (and therefore removal) of As(V) with biochar. Recent published work can provide detailed discussion on SIP and the used experimental set-up [3,51]. In brief, three laboratory columns of 240 mm length and 38 mm diameter, were prepared in accordance with previous work [51]. One column was filled with sand and served as a control, while the other two were filled with BC-500 adjusted sand at 5% and 10% by weight, respectively. The biochar:sand ratio was 7.4:140 and 14.8:132.6 mL respectively for 5% and 10% amended columns. To ensure complete saturation of the columns and avoid flow channeling, the solutions were pumped from the bottom to the top of the columns at a constant flow of 0.16 $\text{mL}\cdot\text{min}^{-1}$ for 16 h. Due to the higher volume required, the concentration of As(V) was kept to 1 mg/L. The SIP technique includes measuring the phase shift (φ) and conductivity magnitude ($|\sigma|$) of an injected current, typically across a wide frequency range, to estimate the real (σ') and imaginary component (σ'') of complex conductivity (σ^*).

$$\sigma^* = \sigma' + i\sigma'', \quad (1)$$

where $i = \sqrt{-1}$

$$\varphi' = \tan^{-1}\left(\frac{\sigma''}{\sigma'}\right), \quad (2)$$

$$\sigma' = |\sigma| \cos(\varphi), \quad (3)$$

$$\sigma'' = |\sigma| \sin(\varphi), \quad (4)$$

The real part (σ') is an electromigration term describing energy loss (conduction), while the imaginary part (σ'') is a charge term, describing energy storage (polarization) [50,55,56].

ICP-OES was used to assess the residual As(V) concentration in eluates collected from the outflow at certain time periods (Plasma Quant 9000). All investigations were carried out in a controlled laboratory setting at a temperature of 23.5 ± 2 °C. Following the 16-h monitoring experiment, the porous media from all columns was collected, and the biochar samples were separated from the sand by sifting due to pore size differences, air-dried, and kept at 4 °C until representative samples were submitted for further investigation.

3. Results and Discussion

3.1. Biochar Characterization

Preliminary screening of the As(V) removal rates for the DPL and the raw biochars after 120 min showed that BC-300 was not effective in removing As(V), whereas BC-500 and BC-800 demonstrated the ability to adsorb As(V) by 15% and 22%, respectively. This can be expected due to greater porous structure formed in biochar produced at higher temperatures, as reviewed by other similar research studies [57]. Therefore, these biochars were then selected for further characterization work by conducting the proximate analysis, while BC-300 was not used due to the low adsorption performance. Table 1 shows the ash content and elemental composition of the feedstock, BC-500 and BC-800 biochars. The ash content and carbon % increased as pyrolysis temperatures were raised. A similar trend was observed in other studies that produced biochar from date-palm waste and generally other studies involving the production of biochar [22,36,58]. However, it is important to highlight that the yield obtained in this study was higher compared to that reported in earlier studies. Usman et al. [59] prepared biochars from date palm leaves and reported a yield of 32.38% at 500 °C and 27.4% at 800 °C. This discrepancy may be due to the additional compaction of feedstock carried out in iron-rods, eliminating voids that can contribute to oxidation and subsequent loss of yield. The organic O content increased at 500 °C; however, it was reduced to 800 °C. This indicates that BC-500 contained a higher concentration of oxygenated functional groups compared to BC-800. The O/C and (N+O)/C ratios are closely connected to the polarity and hydrophobicity of biochar [60]. As these ratios increase, biochar becomes more polar and therefore less hydrophobic. Therefore, BC-500 appears to be more polar and hydrophilic than the original biomass, whereas BC-800 considerably more hydrophobic. This may be due to the stripping of the oxygenated functional groups from the BC-800 surface, as is also indicated by the organic O content values.

Table 1. Basic elemental composition of the biochar produced.

Sample	Yield (%)	Ash (%)	C (wt. %)	H (wt. %)	N (wt. %)	S (wt. %)	O ¹ (wt. %)	Atomic H/C	Atomic O/C	Atomic (N+O)/C
Date palm leaves	-	8	48.97	5.28	2.89	0.56	31.16	1.29	0.47	0.52
BC-500	79	11.7	50.19	2.80	1.80	0.26	33.51	0.66	0.49	0.53
BC-800	48	26	55.40	1.12	1.12	0.0	30.95	0.24	0.41	0.43

¹ Calculated as the difference of 100—(C + H + N + S + ash).

The XRD profile (Figure 1) reveals information about the structure of the raw biochar and the Fe-modified derivative. When a substance is crystalline, well-defined peaks can be observed, whereas non-crystalline or amorphous materials exhibit hollow peaks [61]. The broad reflection at $2\theta = 20\text{--}25^\circ$ is indicative of amorphous biochar and is consistent with other unmodified biochars of poor crystallinity reported in the literature [61,62]. In the pattern corresponding to Fe-BC-500, the intense peak at $2\theta = 23.3^\circ$ corresponds to the (110) plane of α -FeOOH, whereas the peak at $2\theta = 25.5^\circ$ is attributed to the (012) plane of α -Fe₂O₃ [63]. The major peak at $2\theta = 35.45^\circ$ corresponds to the crystalline plane with a Miller index of (311). Other peaks of lower intensity include $2\theta = 30.10^\circ$ (220), 43.10° (400), 53.45° (422), 56.98° (511), and 62.57° (440), matching the standard diffraction patterns of Fe₃O₄ [27]. Therefore, it appears that the preparation methodology deposited various forms of Fe on the biochar surface.

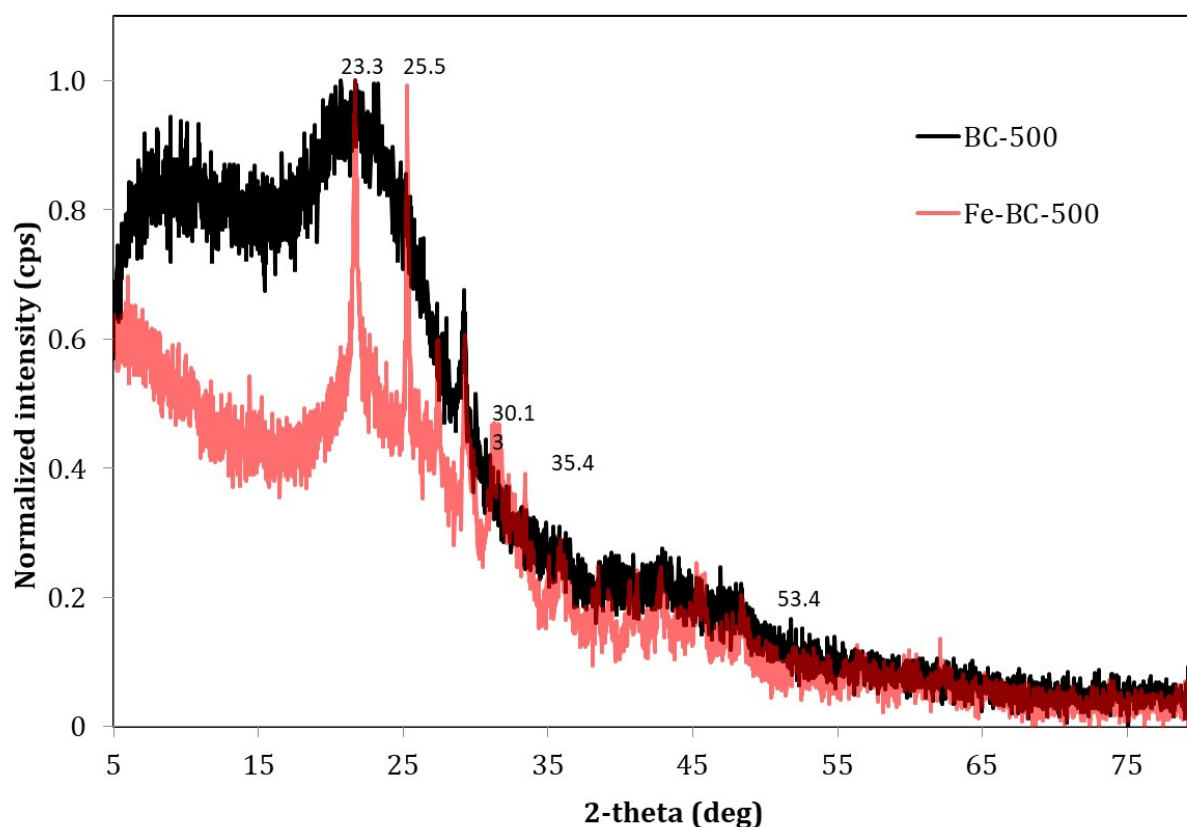


Figure 1. X-ray diffraction (XRD) patterns of BC-500, Fe-BC-500 before As(V) adsorption.

As shown in Figure 2, the SEM images confirmed the porous structure for biochar. Figure 2a,b indicate uniform morphology, and horizontally stretched pores for both BC-500 and BC-800. This trend is generally observed in other studies that produced biochars from biomasses at temperatures exceeding 500 °C [58,64,65]. The post-adsorption image of Fe-BC-500 shows coverage of the surface in a form of a smooth layer that may inhibit adsorption, as active sites are saturated. The structure after adsorption is amorphous and morphologically less favorable for further interaction with As ions. The surface covering may alter biochar's surface properties, which in turn could impact the electrical double layer (EDL) leading to measurable SIP changes, expressed primarily as changes in the imaginary component.

3.2. Adsorption Study

Fe-modified biochars (Fe-BC-500 and Fe-BC-800) demonstrated significant sorption capacity towards arsenic. The comparison between the raw and modified biochar samples can be seen in Figure 3. Modification with Fe played a critical role in adsorption, resulting in considerably higher As removal by the Fe-modified biochars. After 30 min, Fe-BC-800 achieved the highest As(V) removal of 77.8%. However, after 120 min, both Fe-BC-800 and Fe-BC-500 removed 74.1% and 75.8% of As, respectively. Since the performance of these samples was comparable at this time, Fe-BC-500 was considered as the optimum sample due to the lower preparation temperature in pyrolysis and higher yield achieved. Subsequent tests (effect of dosage and pH) were performed with Fe-BC-500 only. The interactions of Fe-functionalized carbonaceous materials with As have been widely researched and described in the literature [66,67]. Although a two-step sorption process of As(V) oxyanion on iron oxide hydroxide based on the production of monodentate and bidentate complexes has been proposed; electrostatic interactions such as H-bonding and pH-dependence also play a role in the adsorption process.

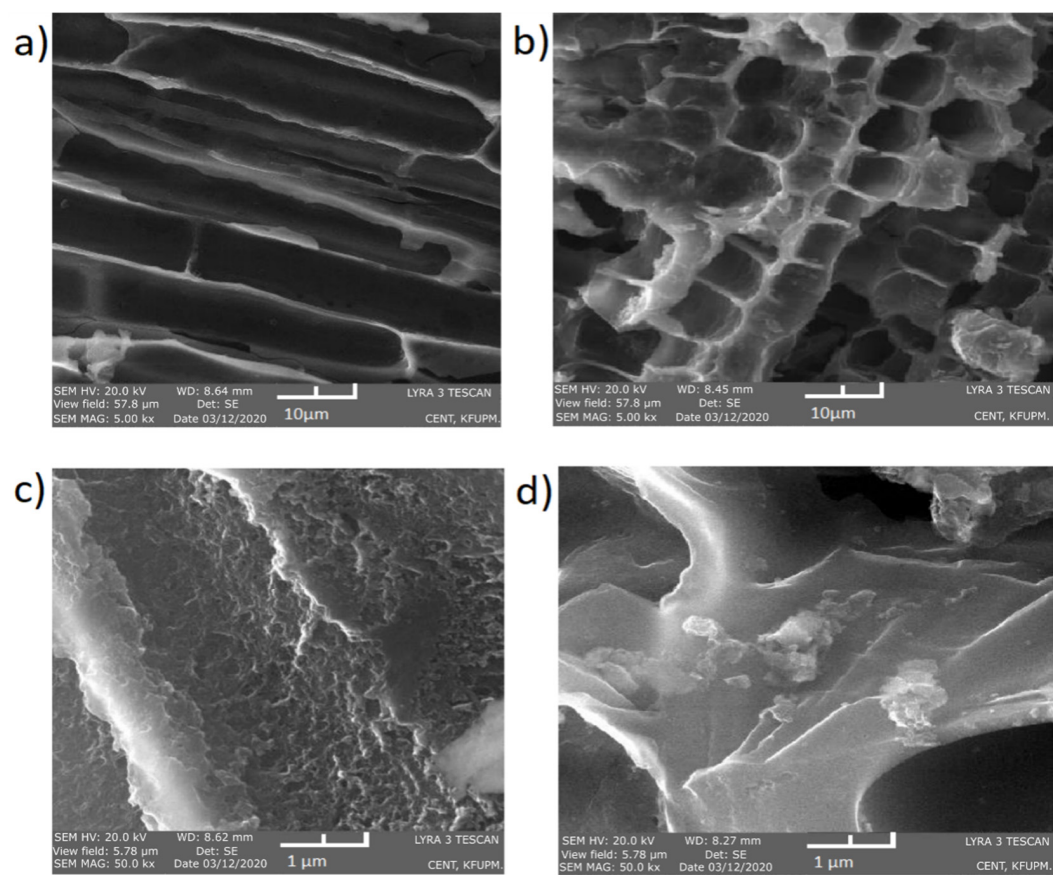


Figure 2. Scanning electron microscopic images of (a) BC-500, (b) BC-800, (c) Fe-BC-500 before adsorption and (d) Fe-BC-500 after adsorption. Fe-BC images show the formation of inhomogeneous Fe layers that are not present in the initial biochar.

It could be considered that the adsorption rate would be proportional to the biochar dosage. However, the adsorption rate (Figure 4a) shows a rapid increase from 2 to 4 g/L dosage, followed by an almost stable rate to 8–12 g/L and a slight increase after that. Considering the efficient use of biochar and that a higher biochar dosage could lead to agglomeration of biochar particles beyond a threshold value, 4 g/L was selected as the optimal dosage for adsorption experiments.

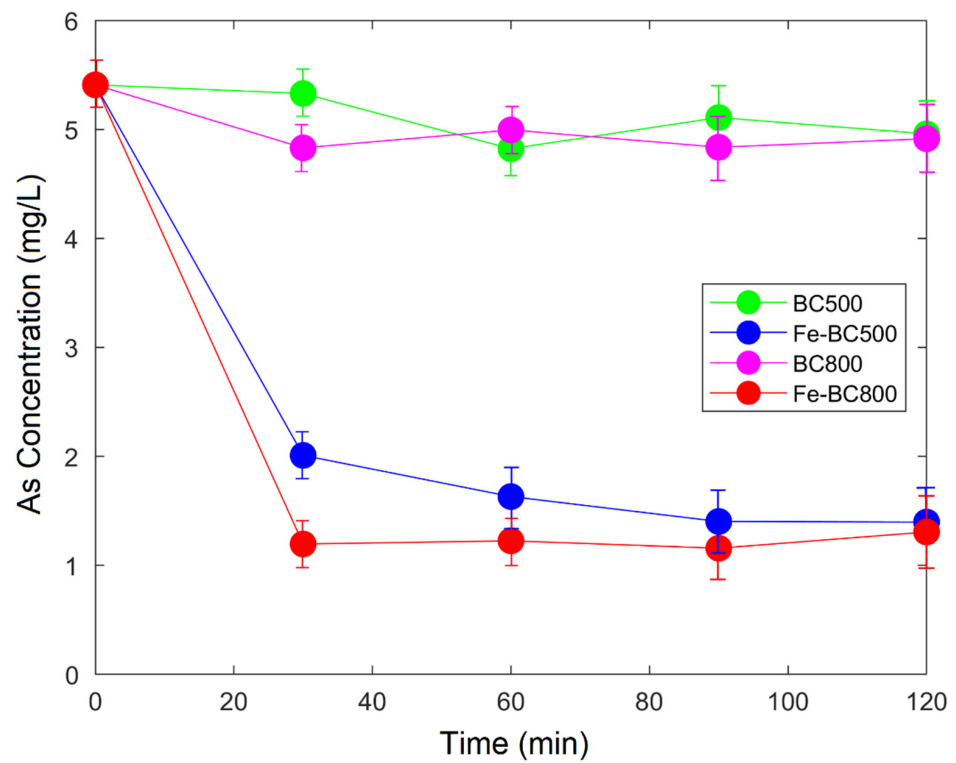


Figure 3. Arsenic sorption of raw and Fe-modified biochar produced at 500 °C and 800 °C through an ICP-OES spectrometer. The tests were conducted on an automatic shaker at 200 rpm under 23 °C temperature for two hours. 0.2 g adsorbent was added in 50 mL volume for an initial concentration of As of 5 mg/L and pH 7.

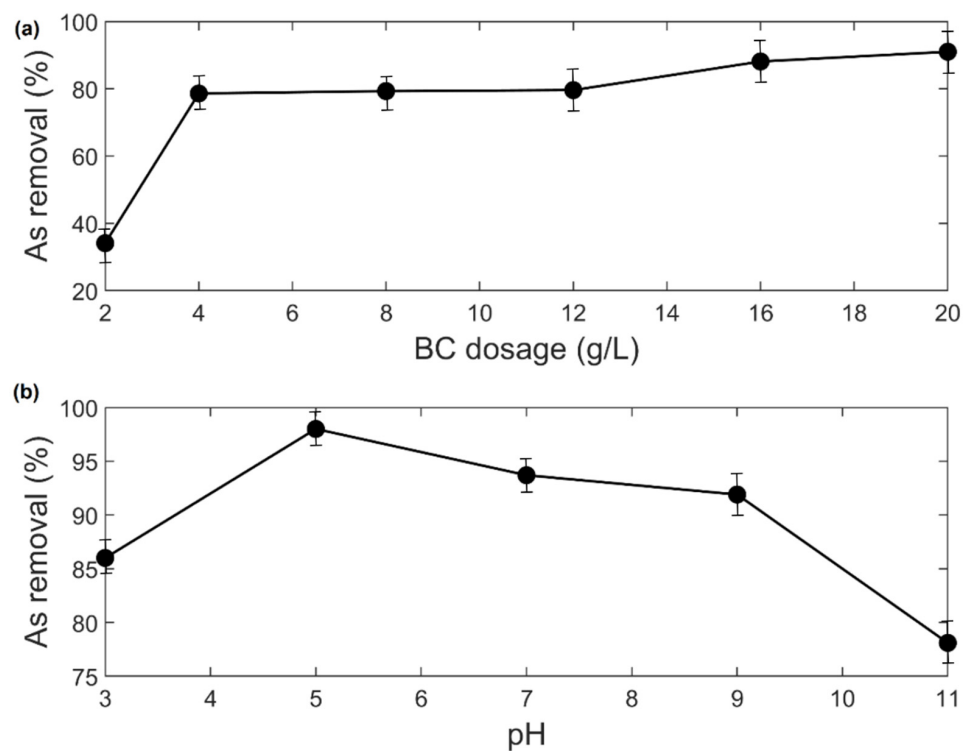


Figure 4. Effect of (a) Fe-BC-500 dosage and (b) pH on As(V) adsorption. Initial As(V) concentration was 5 mg/L, pH 7 (for the effect of dosage) and biochar dosage 4 g/L (for the effect of pH).

Variation in pH influences the presence of surface charge on the adsorbent, which in turn determines the degree of electrostatic attraction. Figure 4b presents the removal of 5 mg/L As(V) at various pH (3, 5, 7, 9 and 11) values using Fe-BC-500. The optimal pH value for arsenic sorption was 5, satisfying the regulation limit of 0.2 mg/L with a residual concentration of 0.1 mg/L. Beyond this value, the efficiency drops below 90%. Similar results have been reported in other research studies [26,43]. It is known that As is classified into various species such as H_3AsO_4 , H_2AsO_4^- , HAsO_4^{2-} , and AsO_4^{3-} depending on the initial pH. Considering the distribution of As species according to pH, H_2AsO_4^- is the main species at pH 3–6, whereas HAsO_4^{2-} and AsO_4^{3-} are the main species at pH 6–8 [68]. At lower pH values, the surface of the adsorbent is protonated by sufficient hydrogen ions [69]. Although the point of zero charge (pH_{pzc}) was not measured for Fe-BC-500, it can be suggested that the surface of Fe-BC-500 is positively charged in the pH region of 4.5–5.5, therefore electrostatic interaction occurs between the positively charged surface of Fe-BC-500 and anionic As species. At the optimum pH 5, 98% of arsenic was removed and further experiments for determining adsorption isotherms were conducted, by adjusting the initial pH to 5.

Tests at different stirring rates were also performed. As shown in Figure 5, a stirring rate of 100 rpm was insufficient to achieve effective As adsorption, whereas gradually increasing the stirring rate to 250 rpm, increased As(V) removal by more than 20% (from 72.6 to 93.2%). Higher stirring rates increase the frequency of contact between adsorbate molecules and the surface groups of carbonaceous materials and therefore reduce the required time to achieve equilibrium. However, it has been reported that stirring rates beyond 250 rpm do not affect the removal efficiency of As sorption [70].

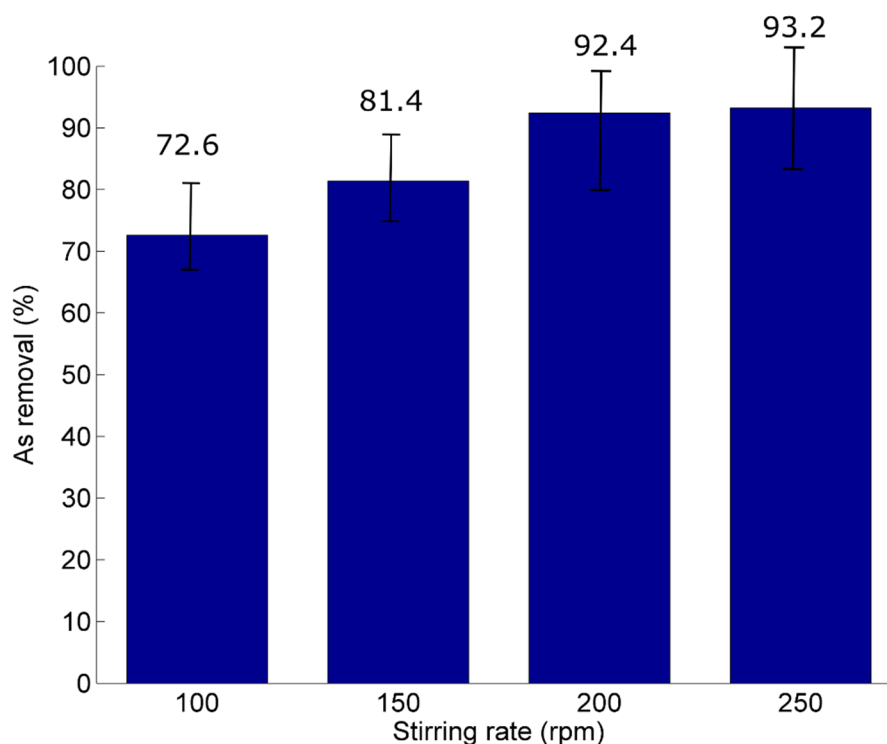


Figure 5. Effect of stirring rate using Fe-BC-500.

The FTIR spectra of BC-500, Fe-BC-500 (before sorption) and Fe-BC-500 (after sorption) are presented in Figure 6. In the single bond region ($2500\text{--}4000\text{ cm}^{-1}$), the broad band at 3375 cm^{-1} corresponding to the stretching vibration of the --OH group, was increased, an observation also made by other researchers. This is due to the formation of As(OH)_3 , which adsorbs weakly at the water–magnetite interface through a network of hydrogen-bonded interactions with water molecules on the surface of the adsorbent [71,72]. The band at

2978 cm^{-1} is due to the asymmetric/symmetric stretch of the methyl C-H bond. In the double bond region (1500–2000 cm^{-1}), the band at 1578 cm^{-1} is attributed to the carboxylate anion (RCOO^-), whereas the band at 1377 cm^{-1} is attributed to the asymmetric/symmetric bend of the methyl C-H bond. The band at 1111 cm^{-1} corresponds to the C-O stretch of secondary alcohols [73]. The band at 787 cm^{-1} —observed at the Fe-BC-500 after As adsorption—may be attributed to the As-O bond, thus confirming the presence of As on the Fe-BC-500 surface [74]. The sharp band at 565 cm^{-1} is characteristic of the vibration of the Fe-O bond [42].

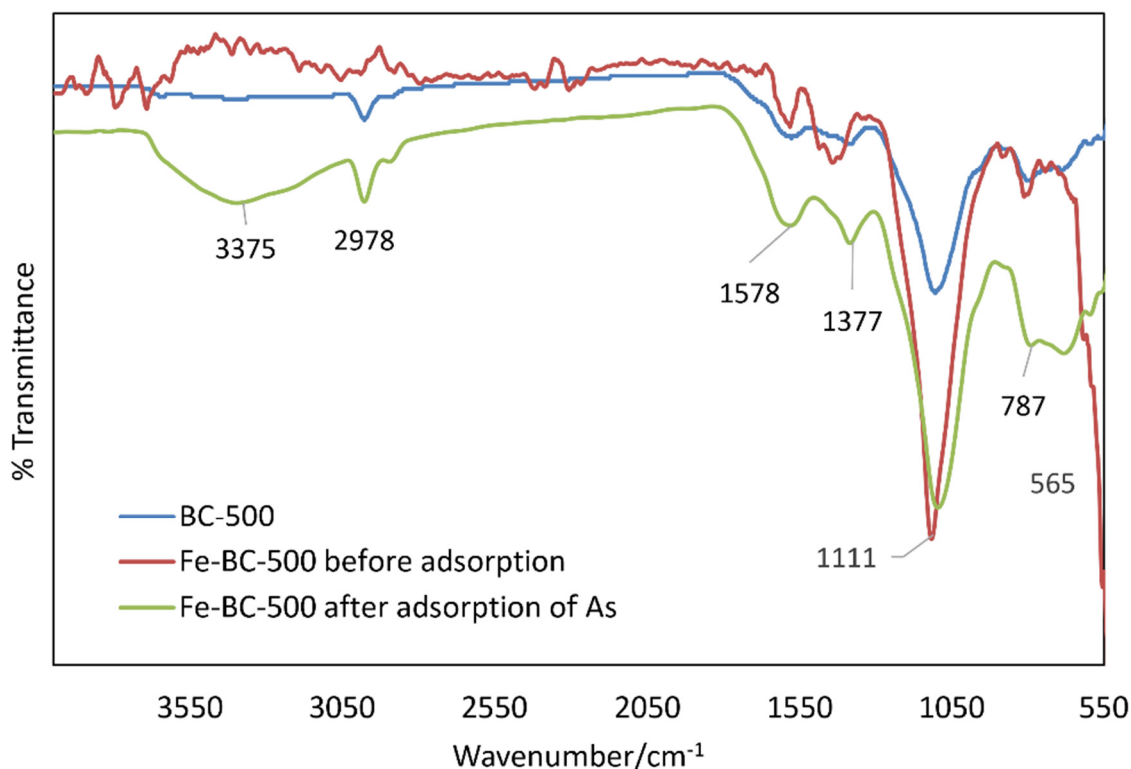


Figure 6. FTIR adsorption spectrum of BC-500, Fe-BC-500 before As(V) adsorption and Fe-BC-500 after As(V) adsorption.

Adsorption isotherms describe the equilibrium performance of adsorbents and are usually used for characterization of the porous solids as well as designing the adsorption process at a larger scale. The experimental data were fitted into the Langmuir and Freundlich model isotherms and the results are shown in Table 2. Both the Langmuir and Freundlich isotherms model described the adsorption process satisfactorily. Therefore, it can be suggested that adsorption of As on Fe-BC-500 was a combination of monolayer (Langmuir) and heterogeneous multi-layer (Freundlich) processes. Taking into account the SEM observations, it may be suggested that As interacted with the inhomogeneously deposited clusters of Fe_3O_4 in addition to any interactions with functional groups on the Fe-BC-500 surface [75]. A comparison to other adsorbents highlights the dependency of As adsorption on the solution pH and leads to the conclusion that additional parameters should be taken into account before scale-up, such as the cost of adsorbent production and recyclability. Kinetic analysis of the adsorption of As on Fe-BC-500 revealed that the process follows the pseudo-2nd order model ($K_2 = 0.8 \cdot 10^{-5}$, $q_e(\text{mg/g}) = 4.3$, $R^2 = 0.96$), rather than the pseudo-1st order model ($K_1 = 0.0107$, $q_e(\text{mg/g}) = 4.02$, $R^2 = 0.80$). This observation agrees well with earlier studies of As adsorption on various carbonaceous adsorbents [27,76].

Table 2. Parameters of the Langmuir and Freundlich isotherm models and comparison of the Q_{\max} value with the published literature are presented.

Adsorbent	Langmuir			Freundlich		
	Q_m (mg/g)	K_L (Lg ⁻¹)	R^2	n	K_F (mg ¹⁻ⁿ g ⁻¹ L ⁿ)	R^2
Fe-BC-500	0.962	3.42	0.85	54.3	6.91	0.89
Q_m (mg/g) values of other adsorbents						
Fe-bamboo biochar, pH 7, 25 °C [76]	49			Magnetic pinewood biochar, pH 7 [77]		0.3
Fe-hickory biochar, pH 5.8 [78]	22			Zero valent iron switchgrass biochar, pH 7–7.5 [79]		7.9
Tea waste magnetic porous carbonaceous, pH 5 [80]	38			Iron impregnated biochar, pH 3 [81]		14.7

3.3. SIP Monitoring

Both 5% and 10% Fe-BC-500 modified columns successfully removed As(V) from wastewater of initial concentration 1 mg/L and residual concentrations 0.0129 and 0.0187 mg/L respectively. When compared to the reference column, both biochar-amended columns obtained high removal up to 98%, while the reference column removed 17%. The control column showed a shallow decrease in the first 4 h and a slight increase afterward, compared with the biochar amended columns, followed by no change over the duration of the experiment probably related with required saturation of the not conductive sand used. The biochar-amended columns showed no discernible change. As a result, the 5% Fe-BC-500 is the most efficient under our testing conditions. Although a higher biochar concentration would imply a greater number of active sites and functional groups accessible to interact with As(V), particle aggregation in the column might cancel out any more adsorption sites, even lowering the overall number of available sites [33,51].

The SIP response (real and imaginary conductivity) appeared to be heavily influenced by As(V) adsorption (Figure 7). The higher real conductivity of 10% Fe-BC-500, compared to 5% Fe-BC-500, is explained by the contribution of the higher concentration of biochar itself. The real conductivity dropped significantly after 4 h, attributed to the fast removal of As(V) ions (lowering bulk conductivity) due to adsorption on biochar surface, followed by a smaller drop after 5 h, until the end of the experiment. The imaginary conductivity of 10% Fe-BC-500 during the first hour is also slightly higher than the 5% Fe-BC-500 amended column, possibly associated with higher surface area [82], suggesting that SIP can be used to quantify biochar content in porous media. Similarly, the imaginary conductivity appears to follow a similar pattern. Increased imaginary conductivity for 10% Fe-BC-500 may also be attributed to membrane polarization, which is prevalent in porous media with pore constrictions and high cation exchange capacity (CEC) [83–85]. SIP measurements were taken in the 0.01–10 kHz frequency range. We focused on the 10 Hz frequency (Figure 7) to better comprehend the temporal nature of SIP because it appeared as a first moderated peak in both data, although other frequencies (up to 100 Hz) revealed comparable tendencies. The actual conductivity data corroborated the As effluent monitoring.

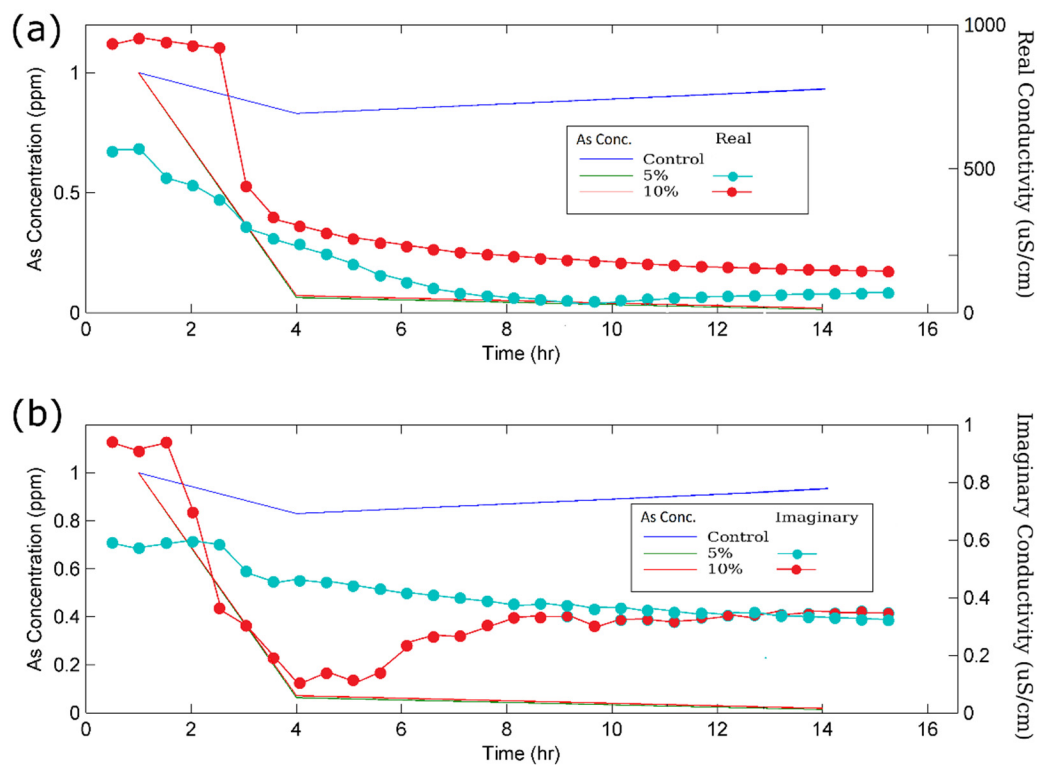


Figure 7. (a) Real and (b) imaginary conductivity of 5% and 10% Fe-BC-500 amended columns for the duration of the experiment (10 Hz) compared with As concentrations (mg/L) are shown. Control As concentration (mg/L) is also presented, while the SIP response of the control column is truncated in order to increase the scale contrast between 5% and 10% Fe-BC-500 results. Initial As(V) concentration was 1 mg/L and pH 5.

SIP could offer a long-term monitoring solution, providing real-time information on the biochar-based adsorption process. The correlation of the SIP parameters (real and imaginary conductivity) to the interactions (and therefore removal) of the As(V) with biochar, can advance current efforts for quantitative interpretation of geophysical signals, along with developing new research opportunities for remediation approaches. For example, the findings of this work can be translated to real-time monitoring advancements of other environmental processes, such as soil remediation and/or anaerobic digestion of bio-waste. In the environmental engineering field, assessing the efficiency of a natural adsorbent (biochar) for the removal of harmful contaminants from the environment is critical. The proposed SIP technology is expected to provide a fast, economic and efficient technology to do so.

Although our results show that SIP responses follow the general trend in the interactions between As and the Fe-functionalized biochar; further investigation of experimental parameters, such as pH dependency, H-bonding, and particle size distribution ash content, is required to explore the links between the SIP responses and the sorption processes to provide insight on which mechanism is dominant.

4. Conclusions

This work demonstrated the utilization of date palm leaves for the production of biochar and its subsequent application as adsorbent of As(V) in aqueous solutions. Given the large quantities of date palm tree residues that end up in landfills in Middle Eastern countries, alternative exploitation strategies are important. The Fe-modified biochar derivative, prepared at the temperature of 500 °C, exhibited the highest adsorption performance at pH 5. The Fe-BC dosage of 4 g/L was determined as the optimum, whereas stirring rates higher than 200 rpm were necessary to achieve a reduction in As concentration from

5 to 0.1 mg/L at pH 5. The real-time monitoring indicated that even over a relative short experimental time (16 h) the SIP signal (real and imaginary component) was consistent with As(V) removal as confirmed by chemical analysis. The SIP signal showed a continuous gradual decrease, that almost reached a plateau at the end of the experiment. However, the imaginary component of 10% showed a different behaviour, with a dramatic drop early on (influenced by the real component changes), followed by an increasing trend with a reducing rate of increase. This dominant signal, after 5 h, was probably related to the higher availability of As sorption sites that resulted in larger changes in the BC surface properties. Such a multi-disciplinary approach has not been applied on As wastewater treatment before, and although more research is needed to establish conclusive links, we hope that we will contribute to discovering a complete, consistent unified model, which will include all the individual theories and will not contain arbitrarily selected parameters that regulate its ex-post agreement with the data of the observations. Combining the use of the SIP method's sensitivity to the interfacial conductivity and adsorption characteristics of biochar opens up new avenues for cost-effective and efficient wastewater treatment monitoring. SIP is a promising method that could address most of the shortcomings that prevent biochar's wide application in environmental management. In contrast to all existing biochar characterization methods, SIP does not require physical sampling, is rapid, and provides information about the investigated volume (in contrast to point sampling and analysis).

Author Contributions: Conceptualization, B.T. and P.S.; methodology, B.T., P.S., D.N.; software, P.K.; validation, B.T., D.K., D.N., P.K. and P.S.; formal analysis, O.M.S. and P.K.; investigation, O.M.S.; resources, B.T., P.S.; data curation, O.M.S.; writing—original draft preparation, P.K., D.K. and D.N.; writing—review and editing, B.T., P.K., D.K., D.N. and P.S.; visualization, P.K.; supervision, B.T., P.S.; project administration, B.T.; funding acquisition, P.S. All authors have read and agreed to the published version of the manuscript.

Funding: This research was funded by King Fahd University of Petroleum and Minerals (KFUPM) and the Deputyship for Research & Innovation, Ministry of Education in Saudi Arabia, grant number DRI 238 (CIPR 2338).

Institutional Review Board Statement: Not applicable.

Informed Consent Statement: Not applicable.

Data Availability Statement: Not applicable.

Conflicts of Interest: The authors declare no conflict of interest. The funders had no role in the design of the study; in the collection, analyses, or interpretation of data; in the writing of the manuscript, or in the decision to publish the results.

References

1. Ouda, O. Domestic water demand in Saudi Arabia: Assessment of desalinated water as strategic supply source. *Desalin. Water Treat.* **2014**, *56*, 2824–2834. [[CrossRef](#)]
2. DeNicola, E.; Aburizaiza, O.S.; Siddique, A.; Khwaja, H.; Carpenter, D.O. Climate Change and Water Scarcity: The Case of Saudi Arabia. *Ann. Glob. Health* **2015**, *81*, 342–353. [[CrossRef](#)] [[PubMed](#)]
3. Siddiq, M.; Tawabini, B.; Kirmizakis, P.; Kalderis, D.; Ntarlagiannis, D.; Soupios, P. Combining geophysics and material science for environmental remediation: Real-time monitoring of Fe-biochar arsenic wastewater treatment. *Chemosphere* **2021**, *284*, 131390. [[CrossRef](#)] [[PubMed](#)]
4. World Health Organization. Arsenic in Drinking-Water. In *Guidelines for Drinking-Water Quality*; WHO Press: Geneva, Switzerland, 2011; ISBN 9789241548151.
5. Merola, R.B.; Hien, T.T.; Quyen, D.T.T.; Vengosh, A. Arsenic exposure to drinking water in the Mekong Delta. *Sci. Total Environ.* **2015**, *511*, 544–552. [[CrossRef](#)]
6. Rodríguez-Lado, L.; Sun, G.; Berg, M.; Zhang, Q.; Xue, H.; Zheng, Q.; Johnson, C.A. Groundwater Arsenic Contamination Throughout China. *Science* **2013**, *341*, 866–868. [[CrossRef](#)]
7. Alidokht, L.; Anastopoulos, I.; Ntarlagiannis, D.; Soupios, P.; Tawabini, B.; Kalderis, D.; Khataee, A. Recent advances in the application of nanomaterials for the remediation of arsenic-contaminated water and soil. *J. Environ. Chem. Eng.* **2021**, *9*, 105533. [[CrossRef](#)]

8. Reeder, R.J.; Schoonen, M.A.A.; Lanzirrotti, A. Metal Speciation and Its Role in Bioaccessibility and Bioavailability. *Rev. Miner. Geochem.* **2006**, *64*, 59–113. [[CrossRef](#)]
9. Pothier, M.P.; Hinz, A.J.; Poulain, A.J. Insights Into Arsenite and Arsenate Uptake Pathways Using a Whole Cell Biosensor. *Front. Microbiol.* **2018**, *9*, 2310. [[CrossRef](#)]
10. Nicomel, N.R.; Leus, K.; Folens, K.; Van Der Voort, P.; Du Laing, G. Technologies for Arsenic Removal from Water: Current Status and Future Perspectives. *Int. J. Environ. Res. Public Health* **2015**, *13*, 62. [[CrossRef](#)]
11. Mudzielwana, R.; Gitari, M.W.; Ndungu, P. Performance evaluation of surfactant modified kaolin clay in As(III) and As(V) adsorption from groundwater: Adsorption kinetics, isotherms and thermodynamics. *Heliyon* **2019**, *5*, e02756. [[CrossRef](#)]
12. Sarkar, A.; Paul, B. The global menace of arsenic and its conventional remediation—A critical review. *Chemosphere* **2016**, *158*, 37–49. [[CrossRef](#)] [[PubMed](#)]
13. Oehmen, A.; Valerio, R.; Llanos, J.; Fradinho, J.; Serra, S.; Reis, M.A.M.; Crespo, J.G.; Velizarov, S. Arsenic removal from drinking water through a hybrid ion exchange membrane—Coagulation process. *Sep. Purif. Technol.* **2011**, *83*, 137–143. [[CrossRef](#)]
14. Pakzadeh, B.; Batista, J.R. Surface complexation modeling of the removal of arsenic from ion-exchange waste brines with ferric chloride. *J. Hazard. Mater.* **2011**, *188*, 399–407. [[CrossRef](#)]
15. Navarathna, C.; Alchouron, J.; Liyanage, A.; Herath, A.; Wathudura, P.; Nawalage, S.; Rodrigo, P.; Gunatilake, S.; Mohan, D.; Pittman, C.; et al. Recent Developments in Aqueous Arsenic(III) Remediation Using Biomass-Based Adsorbents. In *Contaminants in Our Water: Identification and Remediation Methods*; ACS Symposium Series; American Chemical Society: Washington, DC, USA, 2020; Volume 1352, pp. 11–197. ISBN 9780841298941.
16. Yadav, A.; Bagotia, N.; Sharma, A.K.; Kumar, S. Advances in decontamination of wastewater using biomass-based composites: A critical review. *Sci. Total Environ.* **2021**, *784*, 147108. [[CrossRef](#)]
17. Wen, Z.; Lu, J.; Zhang, Y.; Cheng, G.; Huang, S.; Chen, J.; Xu, R.; Ming, Y.-A.; Wang, Y.; Chen, R. Facile inverse micelle fabrication of magnetic ordered mesoporous iron cerium bimetal oxides with excellent performance for arsenic removal from water. *J. Hazard. Mater.* **2020**, *383*, 121172. [[CrossRef](#)] [[PubMed](#)]
18. Srivastav, A.L.; Pham, T.D.; Izah, S.C.; Singh, N.; Singh, P.K. Biochar Adsorbents for Arsenic Removal from Water Environment: A Review. *Bull. Environ. Contam. Toxicol.* **2021**, 1–13. [[CrossRef](#)]
19. Mudzielwana, R.; Gitari, M.W.; Ndungu, P. Enhanced As(III) and As(V) Adsorption From Aqueous Solution by a Clay Based Hybrid Sorbent. *Front. Chem.* **2020**, *7*, 913. [[CrossRef](#)]
20. Siddiq, O.M.; Tawabini, B.S.; Soupios, P.; Ntarlagiannis, D. Removal of arsenic from contaminated groundwater using biochar: A technical review. *Int. J. Environ. Sci. Technol.* **2022**, *19*, 651–664. [[CrossRef](#)]
21. Manyà, J.J. Pyrolysis for Biochar Purposes: A Review to Establish Current Knowledge Gaps and Research Needs. *Environ. Sci. Technol.* **2012**, *46*, 7939–7954. [[CrossRef](#)]
22. Bachmann, H.J.; Bucheli, T.D.; Dieguez-Alonso, A.; Fabbri, D.; Knicker, H.; Schmidt, H.-P.; Ulbricht, A.; Becker, R.; Buscaroli, A.; Buerge, D.; et al. Toward the Standardization of Biochar Analysis: The COST Action TD1107 Interlaboratory Comparison. *J. Agric. Food Chem.* **2016**, *64*, 513–527. [[CrossRef](#)]
23. Guo, M.; Song, W.; Tian, J. Biochar-Facilitated Soil Remediation: Mechanisms and Efficacy Variations. *Front. Environ. Sci.* **2020**, *8*, 183. [[CrossRef](#)]
24. Xiang, W.; Zhang, X.; Chen, J.; Zou, W.; He, F.; Hu, X.; Tsang, D.C.W.; Ok, Y.S.; Gao, B. Biochar technology in wastewater treatment: A critical review. *Chemosphere* **2020**, *252*, 126539. [[CrossRef](#)] [[PubMed](#)]
25. Xie, T.; Reddy, K.R.; Wang, C.; Yargicoglu, E.; Spokas, K. Characteristics and Applications of Biochar for Environmental Remediation: A Review. *Crit. Rev. Environ. Sci. Technol.* **2015**, *45*, 939–969. [[CrossRef](#)]
26. Chen, C.-K.; Chen, J.-J.; Nguyen, N.-T.; Le, T.-T.; Nguyen, N.-C.; Chang, C.-T. Specifically designed magnetic biochar from waste wood for arsenic removal. *Sustain. Environ. Res.* **2021**, *31*, 29. [[CrossRef](#)]
27. Navarathna, C.M.; Karunanayake, A.G.; Gunatilake, S.R.; Pittman, C.U.; Perez, F.; Mohan, D.; Mlsna, T. Removal of Arsenic(III) from water using magnetite precipitated onto Douglas fir biochar. *J. Environ. Manag.* **2019**, *250*, 109429. [[CrossRef](#)] [[PubMed](#)]
28. Park, J.-H.; Lee, J.-H.; Lee, S.-L.; Hwang, S.-W.; Seo, D.-C. Adsorption behavior of arsenic onto lignin-based biochar decorated with zinc. *Colloids Surfaces A Physicochem. Eng. Asp.* **2021**, *626*, 127095. [[CrossRef](#)]
29. Wang, X.; Guo, Z.; Hu, Z.; Zhang, J. Recent advances in biochar application for water and wastewater treatment: A review. *PeerJ* **2020**, *8*, e9164. [[CrossRef](#)]
30. Faheem; Du, J.; Kim, S.H.; Hassan, M.A.; Irshad, S.; Bao, J. Application of biochar in advanced oxidation processes: Supportive, adsorptive, and catalytic role. *Environ. Sci. Pollut. Res.* **2020**, *27*, 37286–37312. [[CrossRef](#)]
31. Pan, X.; Gu, Z.; Chen, W.; Li, Q. Preparation of biochar and biochar composites and their application in a Fenton-like process for wastewater decontamination: A review. *Sci. Total Environ.* **2021**, *754*, 142104. [[CrossRef](#)]
32. Zubair, M.; Ihsanullah, I.; Aziz, H.A.; Ahmad, M.A.; Al-Harathi, M.A. Sustainable wastewater treatment by biochar/layered double hydroxide composites: Progress, challenges, and outlook. *Bioresour. Technol.* **2021**, *319*, 124128. [[CrossRef](#)]
33. Duwiewuah, A.B.; Abubakari, A.H.; Quainoo, A.K.; Amadu, Y. Review of Biochar Properties and Remediation of Metal Pollution of Water and Soil. *J. Health Pollut.* **2020**, *10*, 200902. [[CrossRef](#)] [[PubMed](#)]
34. Pourret, O.; Houben, D. Characterization of metal binding sites onto biochar using rare earth elements as a fingerprint. *Heliyon* **2018**, *4*, e00543. [[CrossRef](#)] [[PubMed](#)]

35. Arevalo-Gallegos, A.; Ahmad, Z.; Asgher, M.; Parra-Saldivar, R.; Iqbal, H.M.N. Lignocellulose: A sustainable material to produce value-added products with a zero waste approach—A review. *Int. J. Biol. Macromol.* **2017**, *99*, 308–318. [[CrossRef](#)] [[PubMed](#)]
36. Rajapaksha, A.U.; Chen, S.S.; Tsang, D.C.W.; Zhang, M.; Vithanage, M.; Mandal, S.; Gao, B.; Bolan, N.S.; Ok, Y.S. Engineered/designer biochar for contaminant removal/immobilization from soil and water: Potential and implication of biochar modification. *Chemosphere* **2016**, *148*, 276–291. [[CrossRef](#)]
37. Anae, J.; Ahmad, N.; Kumar, V.; Thakur, V.K.; Gutierrez, T.; Yang, X.J.; Cai, C.; Yang, Z.; Coulon, F. Recent advances in biochar engineering for soil contaminated with complex chemical mixtures: Remediation strategies and future perspectives. *Sci. Total Environ.* **2021**, *767*, 144351. [[CrossRef](#)]
38. Wang, H.; Tian, Z.; Jiang, L.; Luo, W.; Wei, Z.; Li, S.; Cui, J.; Wei, W. Highly efficient adsorption of Cr(VI) from aqueous solution by Fe³⁺ impregnated biochar. *J. Dispers. Sci. Technol.* **2017**, *38*, 815–825. [[CrossRef](#)]
39. Kumar, R.; Laskar, M.A.; Hewaidy, I.F.; Barakat, M.A. Modified Adsorbents for Removal of Heavy Metals from Aqueous Environment: A Review. *Earth Syst. Environ.* **2019**, *3*, 83–93. [[CrossRef](#)]
40. Wu, C.; Cui, M.; Xue, S.; Li, W.; Huang, L.; Jiang, X.; Qian, Z. Remediation of arsenic-contaminated paddy soil by iron-modified biochar. *Environ. Sci. Pollut. Res.* **2018**, *25*, 20792–20801. [[CrossRef](#)]
41. Godwin, P.M.; Pan, Y.; Xiao, H.; Afzal, M.T. Progress in Preparation and Application of Modified Biochar for Improving Heavy Metal Ion Removal From Wastewater. *J. Bioresour. Bioprod.* **2019**, *4*, 31–42. [[CrossRef](#)]
42. Agrafioti, E.; Kalderis, D.; Diamadopoulos, E. Ca and Fe modified biochars as adsorbents of arsenic and chromium in aqueous solutions. *J. Environ. Manag.* **2014**, *146*, 444–450. [[CrossRef](#)]
43. Georgaki, I.; Soupios, P.; Sakkas, N.; Ververidis, F.; Trantas, E.; Vallianatos, F.; Manios, T. Evaluating the use of electrical resistivity imaging technique for improving CH₄ and CO₂ emission rate estimations in landfills. *Sci. Total Environ.* **2008**, *389*, 522–531. [[CrossRef](#)] [[PubMed](#)]
44. Simyrdis, K.; Papadopoulos, N.; Soupios, P.; Kirkou, S.; Tsourlos, P. Characterization and monitoring of subsurface contamination from Olive Oil Mills' waste waters using Electrical Resistivity Tomography. *Sci. Total Environ.* **2018**, *637–638*, 991–1003. [[CrossRef](#)] [[PubMed](#)]
45. Sparrenbom, C.J.; Åkesson, S.; Johansson, S.; Hagerberg, D.; Dahlin, T. Investigation of chlorinated solvent pollution with resistivity and induced polarization. *Sci. Total Environ.* **2017**, *575*, 767–778. [[CrossRef](#)] [[PubMed](#)]
46. Kessouri, P.; Furman, A.; Huisman, J.A.; Martin, T.; Mellage, A.; Ntarlagiannis, D.; Bucker, M.; Ehosioke, S.; Fernandez, P.; Flores-Orozco, A.; et al. Induced polarization applied to biogeophysics: Recent advances and future prospects. *Near Surf. Geophys.* **2019**, *17*, 595–621. [[CrossRef](#)]
47. Kimak, C.; Ntarlagiannis, D.; Slater, L.D.; Atekwana, E.A.; Beaver, C.L.; Roszbach, S.; Porter, A.; Ustra, A. Geophysical Monitoring of Hydrocarbon Biodegradation in Highly Conductive Environments. *J. Geophys. Res. Biogeosci.* **2019**, *124*, 353–366. [[CrossRef](#)]
48. Ntarlagiannis, D.; Doherty, R.; Williams, K.H. Spectral induced polarization signatures of abiotic FeS precipitation. *Geophysics* **2010**, *75*, F127–F133. [[CrossRef](#)]
49. Ntarlagiannis, D.; Kirmizakis, P.; Kalderis, D.; Soupios, P. Using the spectral induced polarization method to assess biochar performance as a remediation agent. In Proceedings of the AGU Fall Meeting, San Francisco, CA, USA, 12–16 December 2016.
50. Kemna, A.; Binley, A.; Cassiani, G.; Niederleithinger, E.; Revil, A.; Slater, L.; Williams, K.H.; Orozco, A.F.; Haegel, F.-H.; Hördt, A.; et al. An overview of the spectral induced polarization method for near-surface applications. *Near Surf. Geophys.* **2012**, *10*, 453–468. [[CrossRef](#)]
51. Kirmizakis, P.; Kalderis, D.; Ntarlagiannis, D.; Soupios, P. Preliminary assessment on the application of biochar and spectral-induced polarization for wastewater treatment. *Near Surf. Geophys.* **2020**, *18*, 109–122. [[CrossRef](#)]
52. Ben Salem, I.; El Gamal, M.; Sharma, M.; Hameedi, S.; Howari, F.M. Utilization of the UAE date palm leaf biochar in carbon dioxide capture and sequestration processes. *J. Environ. Manag.* **2021**, *299*, 113644. [[CrossRef](#)]
53. Usman, A.R.A.; Abduljabbar, A.; Vithanage, M.; Ok, Y.S.; Ahmad, M.; Ahmad, M.; Elfaki, J.; Abdulazeem, S.S.; Al-Wabel, M.I. Biochar production from date palm waste: Charring temperature induced changes in composition and surface chemistry. *J. Anal. Appl. Pyrolysis* **2015**, *115*, 392–400. [[CrossRef](#)]
54. Din, M.I.; Raza, M.; Hussain, Z.; Mehmood, H.A. Fabrication of magnetite nanoparticles (Fe₃O₄-NPs) for catalytic pyrolysis of nutshells biomass. *Soft Mater.* **2019**, *17*, 24–31. [[CrossRef](#)]
55. Slater, L.D.; Lesmes, D. IP interpretation in environmental investigations. *Geophysics* **2002**, *67*, 77–88. [[CrossRef](#)]
56. Binley, A.; Kemna, A. DC Resistivity and Induced Polarization Methods. *Hydrogeophysics* **2005**, *50*, 129–156. [[CrossRef](#)]
57. Xu, Y.; Xie, X.; Feng, Y.; Ashraf, M.A.; Liu, Y.; Su, C.; Qian, K.; Liu, P. As(III) and As(V) removal mechanisms by Fe-modified biochar characterized using synchrotron-based X-ray absorption spectroscopy and confocal micro-X-ray fluorescence imaging. *Bioresour. Technol.* **2020**, *304*, 122978. [[CrossRef](#)] [[PubMed](#)]
58. Zhao, L.; Cao, X.; Mašek, O.; Zimmerman, A. Heterogeneity of biochar properties as a function of feedstock sources and production temperatures. *J. Hazard. Mater.* **2013**, *256–257*, 1–9. [[CrossRef](#)]
59. Usman, A.; Sallam, A.; Zhang, M.; Vithanage, M.; Ahmad, M.; Al-Farraj, A.; Ok, Y.S.; Abduljabbar, A.; Al-Wabel, M. Sorption Process of Date Palm Biochar for Aqueous Cd (II) Removal: Efficiency and Mechanisms. *Water Air Soil Pollut.* **2016**, *227*, 449. [[CrossRef](#)]
60. Zhao, Z.; Wu, Q.; Nie, T.; Zhou, W. Quantitative evaluation of relationships between adsorption and partition of atrazine in biochar-amended soils with biochar characteristics. *RSC Adv.* **2019**, *9*, 4162–4171. [[CrossRef](#)]

61. Sackey, E.A.; Song, Y.; Yu, Y.; Zhuang, H. Biochars derived from bamboo and rice straw for sorption of basic red dyes. *PLoS ONE* **2021**, *16*, e0254637. [[CrossRef](#)]
62. Keiluweit, M.; Nico, P.S.; Johnson, M.G.; Kleber, M. Dynamic Molecular Structure of Plant Biomass-Derived Black Carbon (Biochar). *Environ. Sci. Technol.* **2010**, *44*, 1247–1253. [[CrossRef](#)]
63. Wang, C.; Liu, H.; Sun, Z.; Huang, J.; Liao, Y. Supported Nanosized α -FeOOH Improves Efficiency of Photoelectro-Fenton Process with Reaction-Controlled pH Adjustment for Sustainable Water Treatment. *Int. J. Photoenergy* **2012**, *2012*, 689807. [[CrossRef](#)]
64. Pongkua, W.; Dolphen, R.; Thiravetyan, P. Effect of functional groups of biochars and their ash content on gaseous methyl tert-butyl ether removal. *Colloids Surf. A Physicochem. Eng. Asp.* **2018**, *558*, 531–537. [[CrossRef](#)]
65. Racek, J.; Sevcik, J.; Chorazy, T.; Kucerik, J.; Hlavinek, P. Biochar—Recovery Material from Pyrolysis of Sewage Sludge: A Review. *Waste Biomass Valorization* **2020**, *11*, 3677–3709. [[CrossRef](#)]
66. Sizmur, T.; Fresno, T.; Akgül, G.; Frost, H.; Moreno-Jiménez, E. Biochar modification to enhance sorption of inorganics from water. *Bioresour. Technol.* **2017**, *246*, 34–47. [[CrossRef](#)] [[PubMed](#)]
67. Benis, K.Z.; Damuchali, A.M.; Soltan, J.; McPhedran, K.N. Treatment of aqueous arsenic—A review of biochar modification methods. *Sci. Total Environ.* **2020**, *739*, 139750. [[CrossRef](#)]
68. Kumar, R.; Kang, C.-U.; Mohan, D.; Khan, M.A.; Lee, J.-H.; Lee, S.S.; Jeon, B.-H. Waste sludge derived adsorbents for arsenate removal from water. *Chemosphere* **2020**, *239*, 124832. [[CrossRef](#)]
69. Niazi, N.K.; Bibi, I.; Shahid, M.; Ok, Y.S.; Burton, E.D.; Wang, H.; Shaheen, S.M.; Rinklebe, J.; Lüttge, A. Arsenic removal by perilla leaf biochar in aqueous solutions and groundwater: An integrated spectroscopic and microscopic examination. *Environ. Pollut.* **2018**, *232*, 31–41. [[CrossRef](#)]
70. Luengo, C.; Puccia, V.; Avena, M. Arsenate adsorption and desorption kinetics on a Fe(III)-modified montmorillonite. *J. Hazard. Mater.* **2011**, *186*, 1713–1719. [[CrossRef](#)]
71. Godlewska, P.; Bogusz, A.; Dobrzyńska, J.; Dobrowolski, R.; Oleszczuk, P. Engineered biochar modified with iron as a new adsorbent for treatment of water contaminated by selenium. *J. Saudi Chem. Soc.* **2020**, *24*, 824–834. [[CrossRef](#)]
72. Dzade, N.Y.; Roldan, A.; De Leeuw, N.H. Structures and Properties of As(OH)₃ Adsorption Complexes on Hydrated Mackinawite (FeS) Surfaces: A DFT-D2 Study. *Environ. Sci. Technol.* **2017**, *51*, 3461–3470. [[CrossRef](#)]
73. Coates, J. Interpretation of Infrared Spectra, a Practical Approach. In *Encyclopedia of Analytical Chemistry*; John Wiley & Sons: Chichester, UK, 2006; Volume 112, pp. 22–31.
74. Sattar, M.S.; Shakoor, M.B.; Ali, S.; Rizwan, M.; Niazi, N.K.; Jilani, A. Comparative efficiency of peanut shell and peanut shell biochar for removal of arsenic from water. *Environ. Sci. Pollut. Res.* **2019**, *26*, 18624–18635. [[CrossRef](#)]
75. Çathıoğlu, F.; Akay, S.; Turunç, E.; Gözmen, B.; Anastopoulos, I.; Kayan, B.; Kalderis, D. Preparation and application of Fe-modified banana peel in the adsorption of methylene blue: Process optimization using response surface methodology. *Environ. Nanotechnol. Monit. Manag.* **2021**, *16*, 100517. [[CrossRef](#)]
76. Alchouron, J.; Navarathna, C.; Chludil, H.D.; Dewage, N.B.; Perez, F.; Hassan, E.B.; Pittman, C.U., Jr.; Vega, A.S.; Mlsna, T.E. Assessing South American Guadua chacoensis bamboo biochar and Fe₃O₄ nanoparticle dispersed analogues for aqueous arsenic(V) remediation. *Sci. Total Environ.* **2020**, *706*, 135943. [[CrossRef](#)] [[PubMed](#)]
77. Wang, S.; Gao, B.; Zimmerman, A.R.; Li, Y.; Ma, L.; Harris, W.G.; Migliaccio, K.W. Removal of arsenic by magnetic biochar prepared from pinewood and natural hematite. *Bioresour. Technol.* **2015**, *175*, 391–395. [[CrossRef](#)] [[PubMed](#)]
78. Hu, X.; Ding, Z.; Zimmerman, A.R.; Wang, S.; Gao, B. Batch and column sorption of arsenic onto iron-impregnated biochar synthesized through hydrolysis. *Water Res.* **2015**, *68*, 206–216. [[CrossRef](#)]
79. Bakshi, S.; Banik, C.; Rathke, S.J.; Laird, D.A. Arsenic sorption on zero-valent iron-biochar complexes. *Water Res.* **2018**, *137*, 153–163. [[CrossRef](#)]
80. Wen, T.; Wang, J.; Yu, S.; Chen, Z.; Hayat, T.; Wang, X. Magnetic Porous Carbonaceous Material Produced from Tea Waste for Efficient Removal of As(V), Cr(VI), Humic Acid, and Dyes. *ACS Sustain. Chem. Eng.* **2017**, *5*, 4371–4380. [[CrossRef](#)]
81. Fan, J.; Xu, X.; Ni, Q.; Lin, Q.; Fang, J.; Chen, Q.; Shen, X.; Lou, L. Enhanced As (V) Removal from Aqueous Solution by Biochar Prepared from Iron-Impregnated Corn Straw. *J. Chem.* **2018**, *2018*, 5137694. [[CrossRef](#)]
82. Fan, Q.; Sun, J.; Chu, L.; Cui, L.; Quan, G.; Yan, J.; Hussain, Q.; Iqbal, M. Effects of chemical oxidation on surface oxygen-containing functional groups and adsorption behavior of biochar. *Chemosphere* **2018**, *207*, 33–40. [[CrossRef](#)]
83. Merriam, J.B. Induced polarization and surface electrochemistry. *Geophysics* **2007**, *72*, F157–F166. [[CrossRef](#)]
84. Titov, K.; Komarov, V.; Tarasov, V.; Levitski, A. Theoretical and experimental study of time domain-induced polarization in water-saturated sands. *J. Appl. Geophys.* **2002**, *50*, 417–433. [[CrossRef](#)]
85. Vinegar, H.J.; Waxman, M.H. Induced polarization of shaly sands. *Geophysics* **1984**, *49*, 1267–1287. [[CrossRef](#)]